# Droplet Sizing Performance of Different Shadow Sizing Codes

**Ralf Kapulla[*], Jenny Tuchtenhagen[**], Armin Müller[**], Klaus Dullenkopf[**], Hans-Jörg Bauer[**]**

[*] Laboratory for Thermal Hydraulics (LTH), Paul Scherrer Institut, 5232 Villigen, Switzerland.

[**] Institute of Thermal Turbomachinery (ITS), University of Karlsruhe, 76131 Karlsruhe, Germany.

**Abstract**

Two shadow sizing codes have been compared using (A) an ideal test target with step-shaped boundary gradients, (B) recorded images of this test target, (C) images taken from a prefilming airblast atomizer and (D) a dense spray dispersed in a carrier gas. The two codes under consideration are an in-house code from the Institute of Thermal Turbomachinery (ITS) and DaVis-SizingMaster Shadow from LaVision. The results of both codes are compared with respect to the number of detected particles, the count mean diameter D(1,0) and the Sauter mean diameter D(3,2). From the target tests it was found that the lower resolution limit of the ITS code enables the detection of particles represented down to one pixel, whereas for the DaVis-code – in line with the technical specification from LaVision – the lower resolution limit corresponds to particles having a diameter of 3 pixels. The results obtained for the case of the airblast atomizer demonstrate a similar detectability, i.e. the number of detected particles in one picture is the same for both codes for low, medium and dense sprays cases. Furthermore, the calculated droplet size distributions are in good agreement with each other, indicating size independent detectability. For the measurements of droplet size distributions in the spray, the count based as well as the cumulative volume size distributions based on the ITS and the DaVis code agreed very well.

## 1 Introduction

The increasing availability of commercial image analysis software for aerosol characterization by means of shadow sizing for spherical as well as irregular shaped particles during the past few years necessitates a comparison of the capabilities and reliability of the different codes. In the present investigation, the performance and limitations of two shadow sizing codes for the analysis of shadowgraphy pictures have been tested in a joint research project between the Laboratory for Thermal-Hydraulics (LTH) at the Paul-Scherrer-Institute, Switzerland, and the Institute of Thermal Turbomachinery (ITS) at the University of Karlsruhe. The two codes under consideration are the commercially available DaVis-SizingMaster Shadow code (V7.2.1) from LaVision (Berg et al. 2006), and an in-house code from the ITS (Müller et al. 2005, Müller et al. 2006) and (Richter et al. 2006).

## 2 Experimental Procedure

The comparison is based on three different test cases. The first, type A test uses a generic test target consisting of 26 rows of 76 dots, each row alternately consisting of increasing or decreasing sized dots. The resulting image is representative of a typical shadow image of a spray, but where number, position and particle diameter are known a priori, Fig. 1, left. The test target was drawn using a graphics program script, with the resulting TIFF image having step-shaped, sharp boundary gradients – simulating an ideal test environment. From this image, a physical test target – type B test – was printed in 5050 DPI on an offset film which was subsequently placed in the focal plane of the recording system, Fig. 1 right. For the synthetic target, the diameters of the opaque disks on each line range from 1 to 76 pixels, in 1 pixel

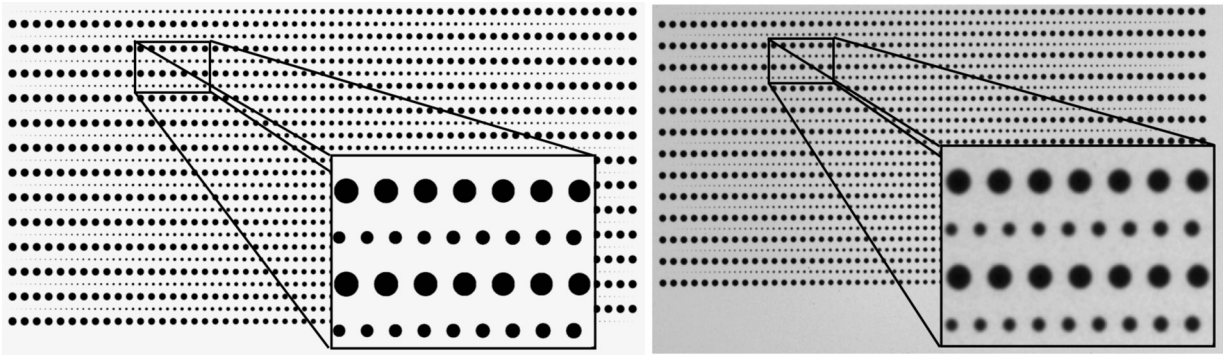

Figure 1: *Synthetic calibration target with 76 particles in each of the 26 rows (left) and image of the printed and recorded calibration target (right).*

increments. With the magnification of the recording system, the disk sizes range from $0.19$ to $14.67$ pixels on the recorded image, in $0.19$ pixel increments, therefore, one pixel on the recorded image corresponds to $25.907$ $\mu m$ on the target; the disk diameters on the target range from $5$ to $380$ $\mu m$. Both test cases contain $26$ disks in each of the $76$ size classes for a total of $1976$ points. Henceforth, in this test case only the target and analysis codes are considered. The recorded target accounts also for imperfect recording conditions with respect to inhomogeneous background illumination, lens aberrations and diffraction limited smooth gradients between particle and background. For the optical setup under consideration, only the near forward scatter light contributes to the shadow image. Shadow images of liquid droplets or opaque disks are thus very similar (Blaisot and Yon 2005).

The second test was conducted with shadow images recorded from the open jet of a prefilming airblast atomizer, (Müller et al. 2006), to asses the performance of both codes for nearly optimal situations with most droplet content within the focal plane – type C test. In contrast to this, in a fourth test, droplet sizes have been measured at different positions in a very dense spray generated by a two fluid atomization, air-assist, full cone spraying nozzle. This setup is characterized by strong optical distortions on both the illumination as well as on the recording side caused by the dense spray, which degrades the image quality considerably – type D test. Finally, the latter droplet measurements are compared with complementary phase-Doppler anemometer (PDA) measurements for the same conditions. The operation principles of the PDA system can be found in (Albrecht et al. 2003). For details of the PDA setup see (Kapulla et al. 2007).

# 3 Analysis Procedure

In general, the analysis of images is a 4-stage process. The first step consists of image preprocessing operations, the second in separating the objects from the background and detecting the different objects in each picture, the third step in calculating the droplet size and the fourth step in different filter operations for the particles detected. These steps will be elaborated on for the DaVis- and ITS-code. The raw pictures treated with DaVis-SizingMaster are filtered with a $3 \times 3$ median filter to reduce noise and to maintain the boundary gradients between object and background. For experimental images, the illumination of the pictures is rarely uniform. The raw image, $G_{raw}$, is therefore subtracted pixel by pixel from a reference image, $G_{ref}$, and the resulting image, $G^*$, is called the inverted image, since the formerly dark droplet shadows now appear in white. This image inversion applies for the type D tests. If weak or no background inhomogenities are present in the image, one has to use a homogeneous white image as a reference, since the treatment with a reference image is mandatory within the DaVis software because the further analysis steps necessitate inverted images. The treatment with a homogeneous white reference image applies for type A to C tests. To separate the objects from the background, the DaVis software uses a simple,

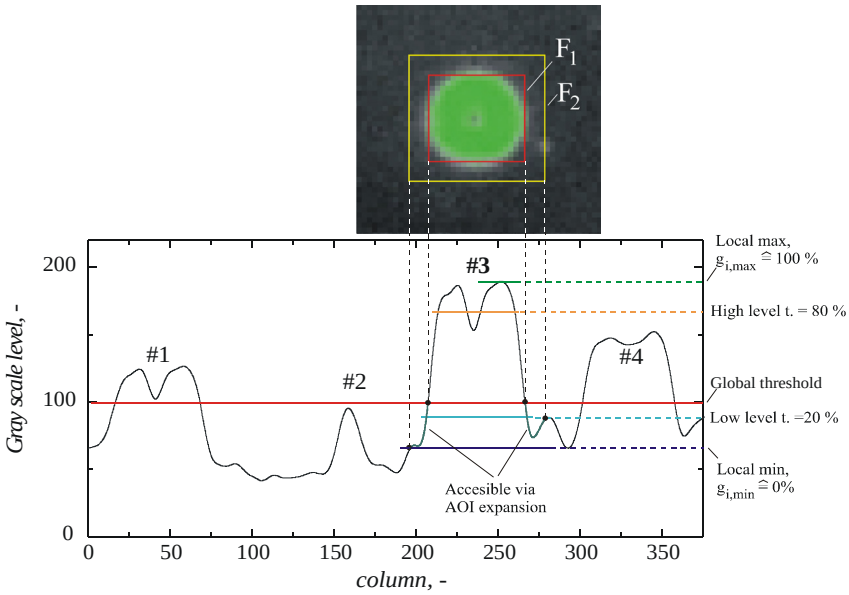


Figure 2: *Local segmentation used by the DaVis software.*

user selected, *global* threshold approach, i.e. this pixel-based segmentation only accounts for the gray values of individual pixel; the surrounding particles are not taken into account. This global threshold is the same for all images of an image series. Since a description of the problems arising from this concept is beyond the scope of this article, the reader is referred to (Kapulla et al. 2007). To determine the particle size, a *local* threshold approach is used as follows: A quadratic bounding box with area $F_1$ encloses each area of pixels with gray levels *above* the global threshold, Fig. 2. The area $F_1$ is expanded with a user-adjustable percentage value (area-of-inter-est (AOI) expansion) and one obtains a bigger area $F_2$. The AOI expansions determines the proximity around the particles for which pixel intensities *below* the global threshold values are also considered. Within areas $F_2$ the *local* maximum, $g_{i,\max}$, and minimum, $g_{i,\min}$, gray values are determined. For the local segmentation, two user selected local thresholds (low level threshold and high level threshold) are used. For the object content segmented with the local high level and low level, two circles with radii $r_l$ and $r_h$ are approximated and the particle diameter is calculated from $d_p = r_l + r_h$, i.e. with this method (i) information below the global threshold is also used to determine the particle diameter and (ii) the mean relative position with respect to the individual particle contrast is always the same.

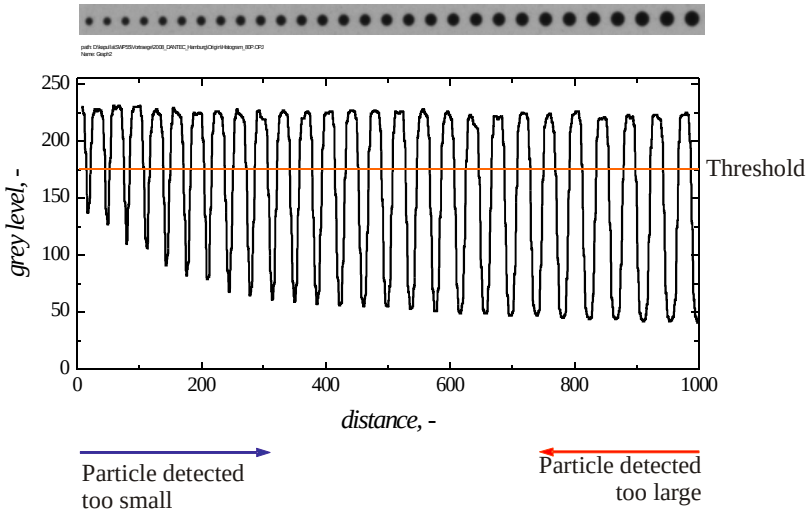


Figure 3: *Qualitative contrast modulation as a function of particle size in conjunction with the relative position between particle representation and a fixed threshold-level.*

In contrast to the DaVis program, the Matlab based ITS-code expects raw images with an already homogeneous background as input, i.e. the particle shadows appear black on a bright background. The global threshold is determined individually as $80\ \%$ from the median of the gray level histogram for each image. This $80\ \%$ value can be adjusted appropriately. Since the ITS-code uses the global threshold not only to distinguish between objects and background, but also for object edge detection, an error occurs in the size calculation. With a fixed threshold, this error is caused by the particle-size-dependent relative

position between particle representation and the threshold-level, Fig. 3, in conjunction with the particle-size dependent contrast modulation. With a fixed threshold-level, small particles with a weak contrast to the background will be measured too small, whereas larger particles with a strong contrast will be measured too large. This makes a calibration mandatory, i.e. based on calibration targets covering the size range of interest, Fig. 1, the difference between measured and true diameter of the particles must be corrected.

# 4 Results

## 4.1 Target Tests

The target tests type-A and -B are used to (i) determine the number of detected particles in each size class (ideally 26) and therefore to quantify the lower resolution limit of the codes. The RMS-value, (ii), within one size class quantifies the precision up to which one code can determine the size. And (iii) the particle-size-dependent deviation of the measured size from the nominal size allows an assessment of the overall precision and, consequently – for the ITS-code – for the correction of the results as explained above and for the DaVis-software for a re-adjustment of the local thresholds. These results from the target tests can be found in Fig. 4.

The number of detected particles as a function of the particle diameter for the synthetic and the recorded target can be found in Fig. 4 a) and b). It is to say that, (i) the y-axis for both graphs just show the low size class range. Furthermore, (ii), as the synthetic calibration slides only contain the gray scale values $0$ and $255$ and the gradients at the edges of the particles are accordingly steep, the different settings of the global thresholds in both programs have no influence on the particle-detection capabilities. For the type-A test it was found that the DaVis software starts to detect particles with a diameter of $3$ pixel – in line with the technical specification of LaVision – and the nominal number of particles within each size class, i.e. 26, are counted from size class $5$ and above. With one pixel corresponding to an area of $26\ \mu m^2$, the same holds for the DaVis-based results for the recorded target. In contrast to this, the ITS-codes also permits the measurement of the smallest possible particles represented by just one pixel. The RMS-value within one size class as a function of particle diameter can be found in Fig. 4 c) and d) for the synthetic and the recorded target. The relatively high RMS-value of up to $0.4$ pixel for the synthetic target for small particle diameters which levels off for larger particles irrespective of the code used, does not indicate a weakness of the codes, but instead indicates a shortcoming of the target generation process. Disks with the same diameter are not always drawn with the same number of pixels for the same circle area; this becomes less severe for larger particles. For both codes, this results in different calculated diameters for disks in one size class and causes a high RMS-value. One would expect RMS- values of $0.1$ pixel, (Brand and Mohr 1994), which is in fact found for the DaVis-based results from the recorded target ($0.1$ pixel corresponds to $2.6\ \mu m$). The ITS-code also shows a good RMS-value of $3\ \mu m$ for the medium-sized particles, whereas the RMS-values for smaller and larger particles located preferentially on the left and right side of the target, Fig. 1, increases considerably. The reason for this behavior is based on remaining weak uncorrected background intensity inhomogenities on the left and right side of the image caused by the recording situation. These inhomogenities were eliminated and the re-calculated RMS-value presented in Fig. 4 d) are slightly below those calculated for the DaVis code. Since the DaVis software uses a second local segmentation step for the particle size calculation and additionally uses local background information, it is more robust with respect to weak background inhomogenities compared to the ITS-code. The deviation of the detected particle diameter from the nominal particle diameter can be found in Fig. 4 e) and f). For the DaVis-based results and the synthetic image, the deviation for the smallest particles is small and approaches quickly zero for increasing particle diameters, i.e. an excellent agreement between measured and nominal diameter is found, Fig. 4 e). The results for the ITS-code show a systematical error of $+0.6$ pixel, independent of diameter. This devia-

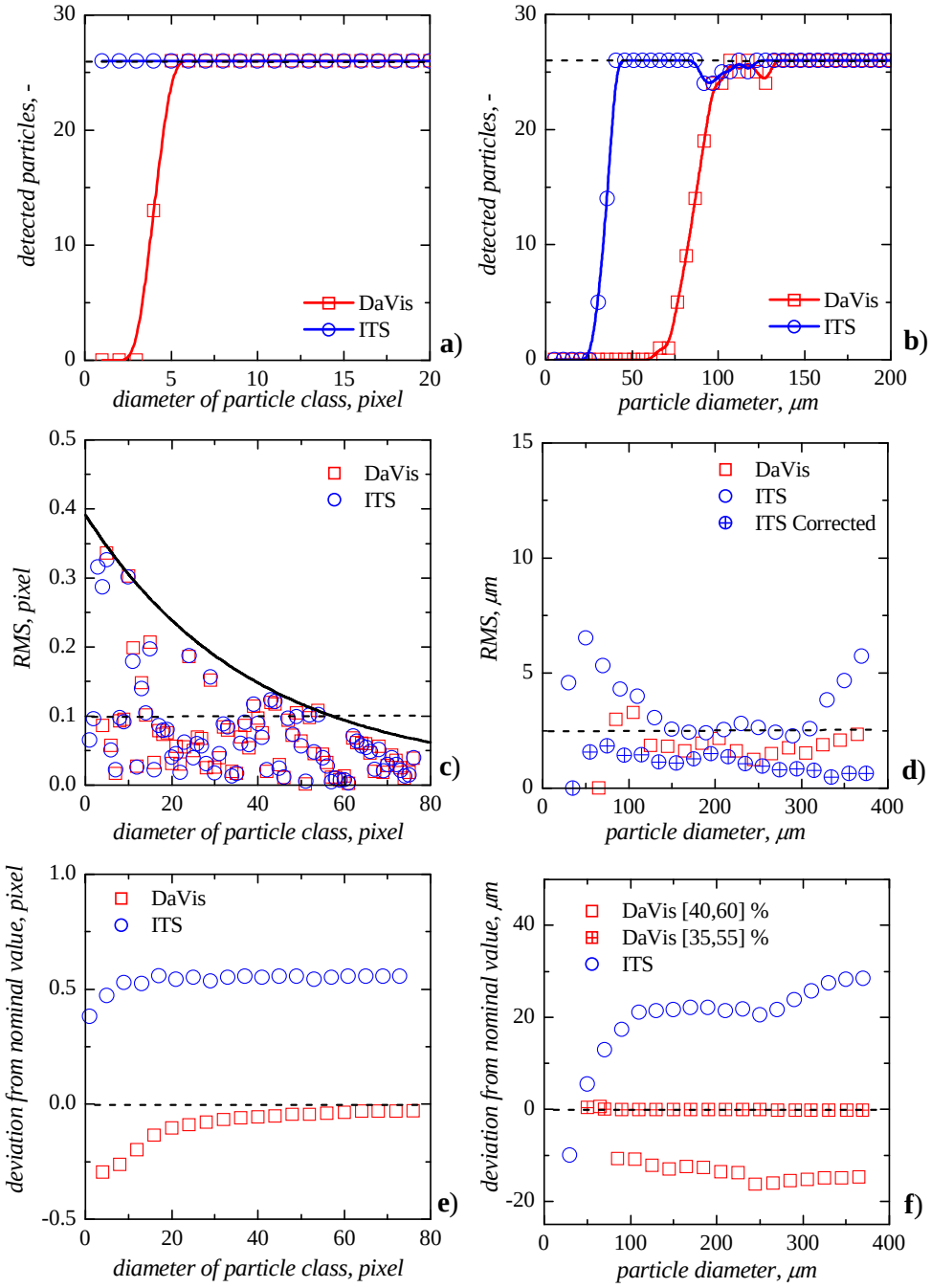


Figure 4: *Results from the synthetic (left) and recorded (right) target tests.*

tion is due to the higher threshold of $80\ \%$ instead of $50\ \%$, which cuts the step-edge intensity profile $30\ \%$ too high, which corresponds to $+0.3$ pixel along the radius. For the recorded calibration target, Fig. 4 f), the ITS-code based results underlie the single-segmentation approach of the code. As already explained above, small particles are measured too small, whereas larger particles with a strong contrast are measured too large. Aiming to improve this deviation and using a global threshold of $50\ \%$ instead of $80\ \%$ simply shifts the ITS result vertically without altering the shape of the graph. This method has the disadvantage that the smallest particles with contrasts which do not exceed the $50\ \%$ threshold will be lost. To solve this problem, Fig. 4 f) must be used as a calibration and the results must be corrected accordingly. For the recorded calibration target, the DaVis-software with default local thresholds of $40$ and $60\ \%$ systematically detects the particles too small, Fig. 4 f). The local thresholds were set to $40\ \%$

and 60 %, respectively, expecting to catch the ´true´ diameter close to the 50 % threshold level, as was done for the 50 % threshold test with the ITS code above. This is in fact true for the disks on the synthetic target, but not for the boundary gradient containing disks of the recorded target. For the recorded target, values of 35 % and 55 % – implicitly expecting the ´true´ diameter at the 45 % level – are more appropriate, Fig. 4 f). It is expected that these values can *not* be generalized and that the appropriate local threshold adjustment is highly dependent on the setup and, therefore, must be determined in-situ for each experiment with a calibration target.

## 4.2 Prefilming Atomizer Tests

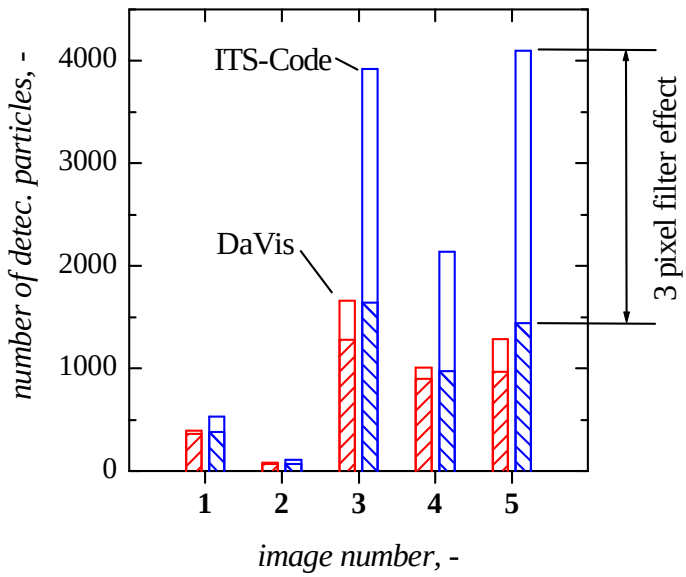


Figure 5: *Number of detected particles for five different operating points of the airblast atomizer tests.*

For the five selected shadow images taken from different operation point of a prefilming airblast atomizer, the number of particles detected on each image are presented in Fig 5. From the calibration target tests, different lower resolution limits were found for the DaVis-software and the ITS-code, respectively. We therefore present – on one hand – the raw results as plain bars and – on the other hand – the normalized results where particles with diameters below 3 pixel and above 25 pixel were neglected, i.e. both codes cover the same size range, with hatched bars. The former tests are referred to as raw results, the latter referred to as filtered results. For the raw results, the ITS-code always counts more particles compared to the DaVis code and for image number 3 to 5, considerably more particles.

Since the ITS-code lowest resolution is below the DaVis-software limit, these particles are preferentially small. For image number 5 for example, the ITS-code counts $\approx$ 4000 particles whereas the DaVis software counts $\approx$ 1000 particles. These small particles have a pronounced effect on the number but not on the overall volume of the particles which, for the case of the prefilming atomizer tests, is dominated by larger particles. For the filtered results, the huge difference between ITS-code and DaVis-software vanishes and the number of detected particles is comparable irrespective of the image used. Using the filtered results, it is possible to calculate the cumulative volume distribution as function of particle size, Fig. 6. For image 1, both codes calculate nearly identical results whereas the

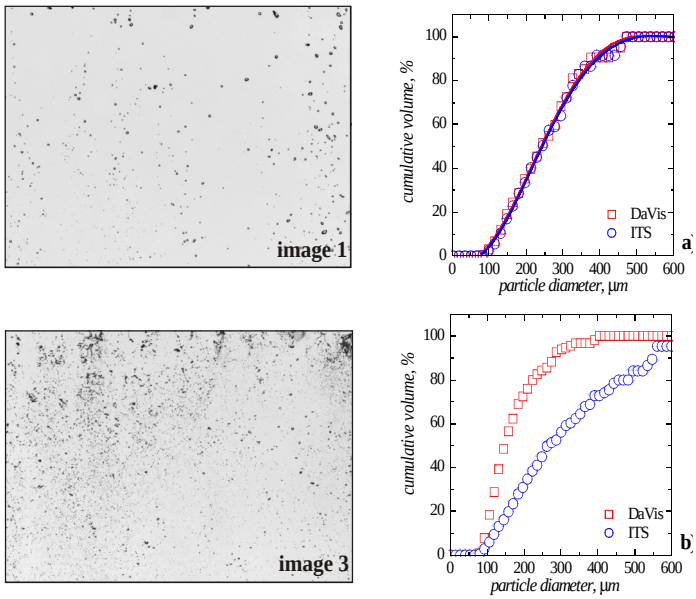


Figure 6: *Shadow images used to test ITS- and DaVis-code (left) and corresponding cumulative volume distribution as a function of particle diameter (right).*

size distribution for image 3 differs due to some larger particles detected by the ITS-code, but not from the DaVis-code. Since larger particles contribute a large volume this becomes immediately apparent in the cumulative size distribution. The higher detectability for the ITS code is caused by elliptical ligaments formed in the vicinity of the prefilming surface.

## 4.3 Spray tests

The spray tests were performed through plane glass windows at three different vertical positions in a cylindrical Perspex tube with an inner diameter of $500\ mm$. The coordinate system has its origin in the symmetry-axis of the test section. The droplets are generated by means of a twin-fluid atomization, air-assist, full cone spraying nozzle projecting upwards in the axis of the test section. The spraying nozzle orifice is located $1.6\ m$ below the measurement position. The droplets generated are transported by a carrier gas through the test section. The cumulative volume distributions measured by means of shadowgraphy and a phase-Doppler anemometry system (PDA) plotted for two horizontal positions (P000 and P200) in Fig. 7. The Shadowgraphy results were analyzed with the DaVis- as well as with the ITS-code. For the DaVis- and ITS-code based results there is an excellent agreement for the cumulative size distributions as well as for the derived count mean diameter, $D(1,0)$ and the Sauter-mean diameter, $D(3,2)$, irrespective of the horizontal position, Fig. 7 a) and b), and irrespective of the droplet-size-distributions generated (not shown). Additionally, for the in-axis position (P000), we find a good agreement with the PDA-based results, whereas there is a considerable difference for the outer positions which is especially reflected by the Sauter-mean diameter, Fig. 7 d).

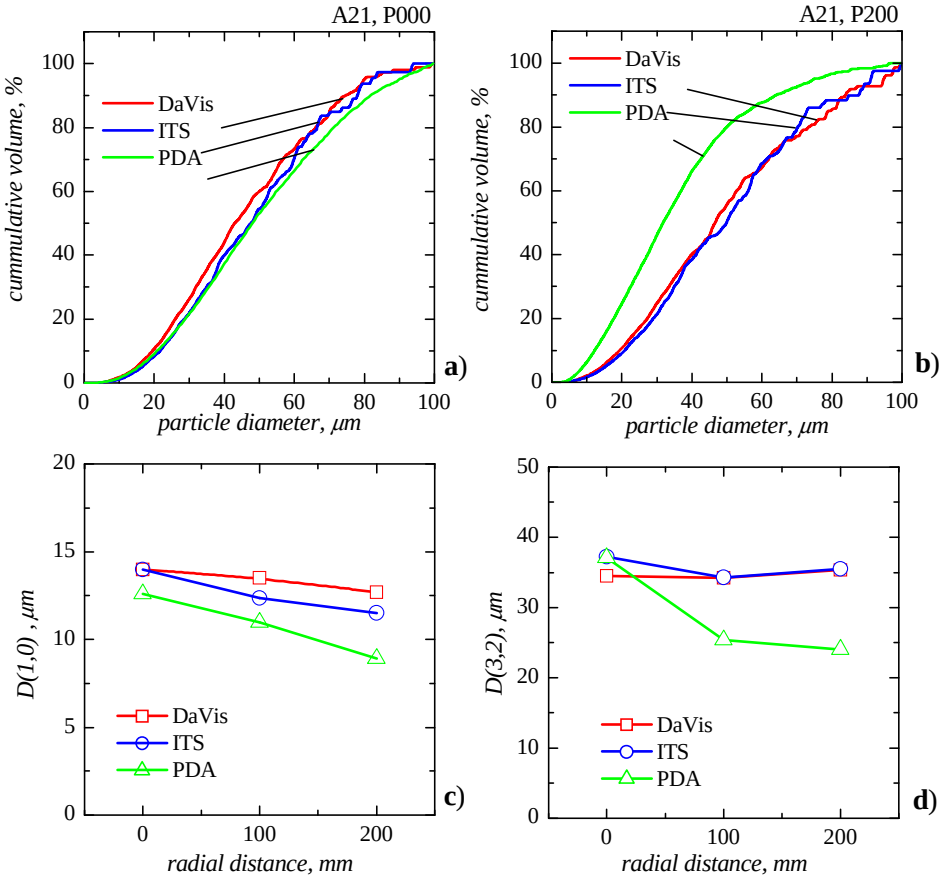


Figure 7: *Cumulative volume distribution at two horizontal measurement positions measured by means of Shadowgraphy and PDA, a) and b), and resulting count mean diameter, D(1,0), and Sauter mean diameter, D(3,2) based on DaVis- and ITS-code as well as on PDA data.*

# 5 Summary

The performance of two image analysis software for aerosol characterization using shadowgraphy images was compared with four different tests. From the target test it was found that the lower resolution limit of the ITS-code permits the measurement of even the smallest possible particles of one pixel, whereas for the DaVis-software the lowest particle detection limit amounts to particles with a diameter of three pixel. With the recorded calibration target it was demonstrated, that the ITS code is less robust with respect to background inhomogenities compared with the DaVis-software and that the local threshold-adjustment in the DaVis-software necessitates the use of calibration targets to adjust for the correct particle diameters. Limiting diameters to the same dynamic range for the two codes, a good agreement for the number of detected particles could be achieved for the prefilming airblast atomizer images. The cumulative size distribution for low-density shadowgraphy images is excellent, whereas this size distribution for high density images differs considerably. The spray based results demonstrate an excellent agreement for the DaVis- and ITS-based results with respect to the cumulative volume size distribution as well as for the count mean and Sauter-mean diameter. The agreement with PDA-based results show a strong position bias, i.e. the comparison in the axis of the test section is good, whereas one finds considerable differences for out-of-axis positions.

# References


Albrecht, H.-E. and Borys, M. and Damaschke, N. and Tropea, C. (2003), Laser Doppler and phase Doppler measurement techniques. Springer-Verlag.

Berg, T., Deppe, J., Michaelis, D. Voges, H. and Wissel, S. (2006), Comparison of particle size and velocity investigations in sprays carried out by means of different measurement techniques, ICLASS-2006, 27. Aug. - 1. Sept., Kyoto, Japan, paper ID ICLASS06-151.

Blaisot, J.B., Yon, J. (2005), Droplet size and morphology characterization for dense sprays by image processing: applications to the Diesel spray, Experiments in Fluids, Vol. 39, pp. 977-994.

Brand, P. and Mohr, R. (1994), Accuracy in image measure, SPIE, Videometrics III, pp. 218-228.

Kapulla, R., Trautmann, M., Sanchez, A. H., Zaragoza, S. C., Hofstetter, S., Häfeli, C. Güntay, S. (2007), Droplet size distribution measurements using phase-Doppler anemometry and shadowgraphy: Quantitative comparison, Lasermethoden in der Strömungsmesstechnik, 15. Fachtagung, Rostock.

Müller, A., Hehle, M., Schäfer, O., Koch, R., Bauer, H.-J. (2005), Zerstäubungsverhalten von Airblastdüsen bei oszillierenden Strömungen, VDI-Bericht Nr. 1888, 22. Deutscher Flammentag, September 21 - 22, Braunschweig, pp. 249-257.

Müller, A., Hehle, M., Schäfer, O., Koch, R., Bauer, H.-J. (2006), Performance of Prefilming Airblast Atomizers in Unsteady Flow Conditions, ASME Turbo Expo 2006, May 8 - 11, Barcelona, Spain.

Richter, B., Dullenkopf, K. Bauer, H.-J. (2005), Investigation of secondary droplet characteristics produced by an isooctane drop chain impact onto a heated piston surface, Exp Fluids, 39:351-363.